analytical chemistry

Article

pubs.acs.org/ac

"Signal-On" Photoelectrochemical Biosensor for Sensitive Detection of Human T-Cell Lymphotropic Virus Type II DNA: Dual Signal Amplification Strategy Integrating Enzymatic Amplification with Terminal Deoxynucleotidyl Transferase-Mediated Extension

Qingming Shen,[†] Li Han,[†] Gaochao Fan,[‡] Jian-Rong Zhang,[‡] Liping Jiang,*[,‡] and Jun-Jie Zhu*[,‡]

[†]Key Laboratory for Organic Electronics and Information Displays and Institute of Advanced Materials, Jiangsu National Synergetic Innovation Center for Advanced Materials (SICAM), Nanjing University of Posts and Telecommunications, Nanjing, Jiangsu 210023, P. R. China

[‡]State Key Laboratory of Analytical Chemistry for Life Science, School of Chemistry and Chemical Engineering, Nanjing University, Nanjing, Jiangsu 210093, P. R. China

Supporting Information

ABSTRACT: A novel "signal-on" photoelectrochemical (PEC) biosensor for sensitive detection of human T-cell lymphotropic virus type II (HTLV-II) DNA was developed on the basis of enzymatic amplification coupled with terminal deoxynucleotidyl transferase (TdT)-mediated extension strategy. The intensity of the photocurrent signal was proportional to the concentration of the HTLV-II DNA-target DNA (tDNA) by dual signal amplification. In this protocol, GR-CdS:Mn/ZnS nanocomposites were used as photoelectric conversion material, while pDNA was used as the tDNA recognizing unit. Moreover, the TdT-mediated extension and the enzymatic signal amplification technique were used to enhance the sensitivity of detection. Using this novel dual signal amplification strategy, the prototype of PEC DNA sensor can detect as low as ~0.033 fM of HTLV-II DNA with a linear range of 0.1−5000 fM, with excellent differentiation ability even for single-base mismatches. This PEC DNA assay opens a promising platform to detect various DNA targets at ultralow levels for early diagnoses of different diseases.

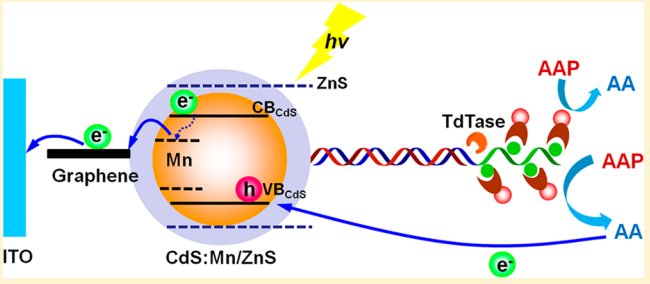

Human T-cell lymphotropic virus type II (HTLV-II) is a human retrovirus closely related to HTLV type I (HTLV-I), which is also a causative agent of adult T-cell leukemia and lymphoma.[1] HTLV-II has significant effect on myelopathy and is also associated with pulmonary and urinary tract symptoms, as well as increased mortality.[2] HTLV-II DNA is present at trace level in clinical samples. Hence, an effective method to realize sensitive detection of this retroviral DNA is necessary.[3] To achieve high sensitivity, various amplification strategies have been developed for sensitive detection of target DNA, such as real-time polymerase chain reaction,[4,5] rolling circle amplification,[6−8] ligase chain reaction,[9] loop-mediated isothermal amplification,[10,11] and other isothermal amplification methods.[12] Although these signal amplification methods are sensitive, some unresolved obstacles still remain, including limited sensitivity, complicated equipment, and a relatively expensive and time-consuming detection procedure. In an attempt to circumvent these problems, Tjong and co-workers introduced a unique DNA polymerization method through DNA polymerase-terminal deoxynucleotidyl transferase (TdT).[13] TdT could catalyze the addition of dUTP to the 3′-OH terminus of the DNA with the length of three or more nucleotides. Unlike the general DNA polymerase, the polymerization mediated by TdT does not require primer as template, thereby presenting a facile, direct, and cost-effective way for DNA labeling and detection.[14]

Among the various detection techniques, photoelectrochemical (PEC) biosensor is a newly developed yet dynamically developing technique for biosensing. Given the separation of excitation source and detection signal, the sensitivity of the PEC biosensor is potentially high and the background signals could be reduced compared with conventional electrochemical and optical methods.[15] Given its simple operation, inexpensive instruments, low background signals, and high sensitivity,[16] the PEC biosensor has attracted a great deal of attention.[17,18] The photo-current conversion efficiency of the PEC biosensor is one of the important parameters for PEC detection sensitivity, which mainly depends on the photoactive materials immobilized on the substrate electrode. Among the various photoactive materials, cadmium sulfide nanoparticles (CdS NPs) have drawn extensive attention because of their unique electronic and optical properties, as well as high PEC activity.[19,20] To

Received: February 17, 2015
Accepted: April 14, 2015

DOI: 10.1021/acs.analchem.5b00679
Anal. Chem. XXXX, XXX, XXX−XXX

Scheme 1. (A) Mechanism of Photocurrent Generation of the HTLV-II DNA PEC Biosensor; (B) Schematic Illustration of the Fabrication Process of the PEC Biosensor

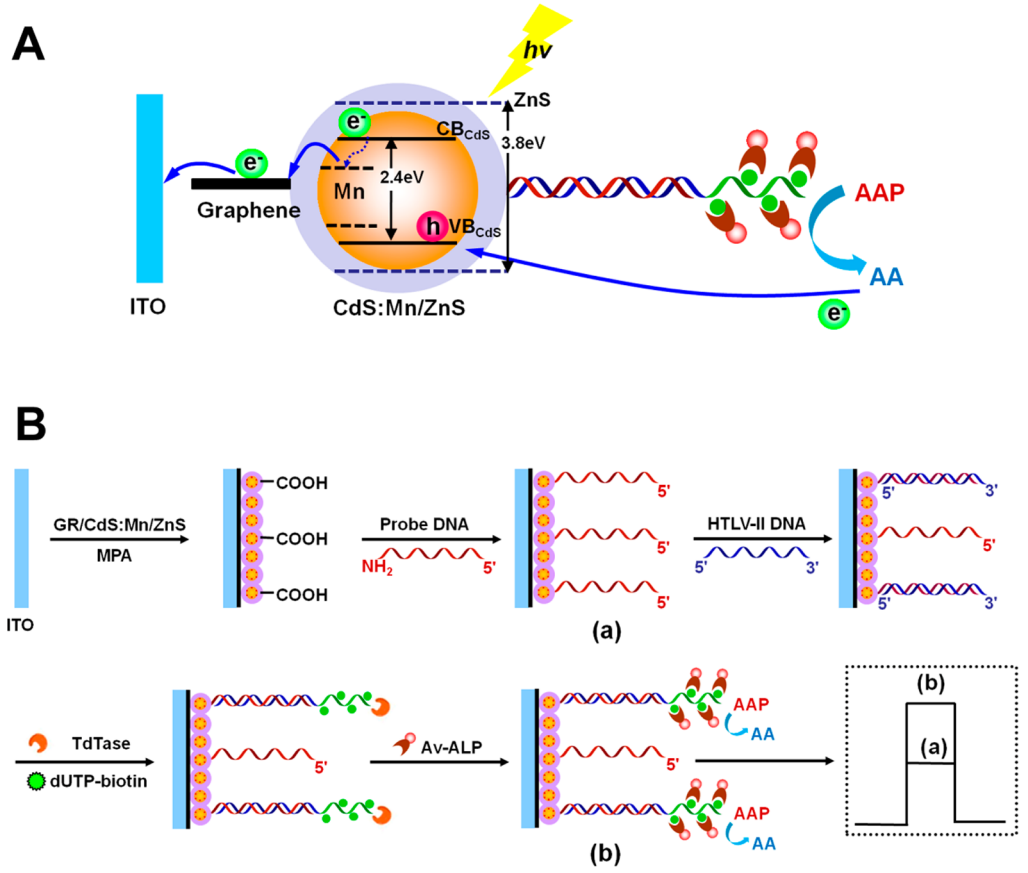

further improve the photoelectric properties of CdS NPs, we fabricated a novel nanocomposite consisting of reduced graphene oxide (GR) and CdS:Mn NPs. The incorporation of GR could enhance charge separation and facilitate charge transport, thereby improving photovoltaic performance. In addition, the high surface area of GR could load more CdS:Mn NPs. The doped Mn^{2+} ion could create an electronic state in the midgap region of CdS that could prompt charge separation, inhibit recombination dynamics, and broaden the wavelength range of light absorption, thereby increasing the photocurrent signals. The ZnS shell, which serves as a passivation layer, could also effectively increase the photocurrent by prohibiting the formation of surface defects on CdS NPs and inhibiting the electron recombination with the redox couple (Scheme 1A).[20] Although the GR-CdS:Mn/ZnS nanocomposites display attractive PEC properties and could be a promising semiconductor material for PEC biosensors, to the best of our knowledge, their application in PEC biosensor has not been reported yet.

Herein, we developed a novel "signal-on" PEC biosensor based on dual signal amplification strategy by TdT-mediated isothermal amplification coupled with enzyme amplification for the detection of HTLV-II DNA (target DNA, tDNA), using GR-CdS:Mn/ZnS nanocomposites as photoactive material. The TdT-mediated extension strategy was introduced into as-fabricated PEC biosensor to amplify the signal. The extension technique utilized the tDNA strand as the primer, without the need to add new DNA sequence as template, which greatly simplified the procedure. As shown in Scheme 1B, after tDNA hybridized with probe DNA (pDNA) on the electrode surface, the multiplex biotinylated dUTP (dUTP-biotin) was sequentially added into the tDNA chain extended by TdT "in situ". Depending on the high exactitude of TdT, multiplex dUTP-biotin was only incorporated into 3′-OH terminal tDNA, thereby reducing the unspecific reaction and yielding a lower background. Furthermore, Scheme 1B also shows that the extended multiplex biotin could conjugate with avidin-alkaline phosphatase (Av-ALP), which could catalyze the hydrolysis of 2-phospho-L-ascorbic acid trisodium salt (AAP) and generate electron donor-ascorbic acid (AA).[20,21] In addition, Scheme 1B clearly illustrates that the Av-ALP conjugated only with the extended biotin labeled DNA chain induced by TdT. In the present detection system, the higher tDNA concentration could lead to more biotin sites, and thus, more Av-ALP could anchor on the extended chains. Given the enzyme amplification of ALP, the photocurrent response could be greatly enhanced by the increased amount of AA generated from the catalytic hydrolysis of AAP by the ALP enzyme. The intensity of the photocurrent signal was proportional to the concentration of HTLV-II DNA by this dual signal amplification strategy. On the basis of the isothermal amplification coupled with enzyme amplification, the proposed PEC system could achieve the highly sensitive and selective HTLV-II DNA detection.

EXPERIMENTAL SECTION

Materials and Reagents. Graphite powder was purchased from J&K Scientific Ltd. Sulfuric acid (H_2SO_4), potassium peroxydisulfate ($K_2S_2O_8$), phosphorus(V) oxide (P_2O_5), potassium permanganate ($KMnO_4$), hydrochloric acid (HCl),

DOI: 10.1021/acs.analchem.5b00679
Anal. Chem. XXXX, XXX, XXX−XXX

manganese acetate tetrahydrate ($Mn(Ac)_2{\cdot}4H_2O$), zinc nitrate hexahydrate ($Zn(NO_3)_2{\cdot}6H_2O$), sodium chloride (NaCl), sodium hydroxide (NaOH), and sodium sulfide (Na_2S) were obtained from Nanjing Chemical Reagent Co. Ltd. (China). Cadmium chloride ($CdCl_2{\cdot}2.5H_2O$) was purchased from Shanghai Chemical Reagent Co. (China). Polyvinylpyrrolidone (PVP, K-30) and 30% hydrogen peroxide (30% H_2O_2) were purchased from Sinopharm Chemical Reagent Co., Ltd. (Shanghai, China). Tris (hydroxymethyl) aminomethane (Tris) and thioacetamide (TAA, ≥99%) were from Lingfeng Chemical Reagent Co., Ltd. (Shanghai, China). 1-Ethyl-3-(3-(dimethylamino)propyl) carbodiimide (EDC), *N*-hydroxysuccinimide (NHS), 3-mercaptopropionic acid (MPA), and 2-phospho-L-ascorbic acid trisodium salt (AAP) were received from Sigma-Aldrich (USA). DNA oligonucleotides, dUTP-biotin, and avidin-alkaline phosphatase (Av-ALP) were purchased from Sangon Biotechnology Co. Ltd. (Shanghai, China). Terminal tansferase (TdT) was obtained from New England Biolabs. Ltd. (Beijng, China). All of the other chemicals were of analytical reagent grade and used without further purification.

The synthetic DNA was purchased from Sangon Biotechnology Co. Ltd. (Shanghai, China) with base sequences as follows:

pDNA (S1): 5'-CTCCCCGACCCAATTTCCACCTTCG -$(CH_2)_6$-NH_2-3';

tDNA (S2): 5'-CGAAGGTGGAAATTGGGTCGGGGAG-3';

One-based mismatch (S3): 5'- CGAAG*A*TGGAAATTGGGTCGGGGAG-3';

Three-based mismatch (S4): 5'- CG*C*AGGTGGAA*T*TTGGGT*A*GGGGAG-3';

Noncomplementary DNA (S5): 5'-GAGGGCCTGCAGGATCATTGGCTTT-3′.

The synthesized oligonucleotides were dissolved in 10 mM Tris−HCl (pH = 7.4, M_{NaCl} = 0.1 M) to desired stock concentrations and stored at −20 °C according to the manufacturer's instructions. The buffer solutions employed in this study are as follows: probe DNA immobilization buffer: 10 mM Tris−HCl, 0.1 M NaCl (pH 7.4); target DNA hybridization buffer: 10 mM Tris−HCl, 0.1 M NaCl, and 20 mM $MgCl_2$ (pH 7.4). The washing buffer was Tris−HCl buffer (10 mM, pH 7.4). Av−ALP was diluted by using 0.1 M PBS buffer containing 0.5% BSA (pH 7.4). Photoelectrochemical determination buffer, 0.1 M PBS (pH 8.0), was prepared by mixing the stock solution of 0.1 M NaH_2PO_4 and 0.1 M Na_2HPO_4, and the pH was adjusted by NaOH or HCl. All aqueous solutions were prepared and diluted using ultrapure water (18.2 MΩ/cm) obtained from the Millipore Milli-Q system.

Apparatus. The morphology and particle size of the samples were characterized by high resolution transmission electron microscopy (HRTEM) (JEOL-2100, Japan). The Cd/Mn ratios of GR-CdS:Mn were characterized by an Oxford INCA detector X-ray spectroscopy (EDX, HORIBA Co.) installed on HRTEM. The UV−visible (UV−vis) absorption spectra were obtained on a UV-3600 UV−visible spectrophotometer (Shimadzu, Japan). Wide-angle powder X-ray diffraction (XRD) patterns were obtained from a Philips X'pert Pro X-ray diffractometer (Cu Kα radiation, λ = 0.15418 nm). Fourier transform infrared (FT-IR) spectra were obtained using a Bruker Vector 22 spectrometer in the frequency range of 4000−500 cm^{-1}. Raman spectra were obtained with a Raman spectrometer (in Via-Reflex, Renishaw, England). Electrochemical impedance spectroscopy (EIS) was performed on an Autolab potentiostat/galvanostat (PGSTAT 30, Eco Chemie B.V., Utrecht, Netherlands) with a three-electrode system in 0.1 M KCl solution containing a 5.0 mM $K_3[Fe(CN)_6]/K_4[Fe(CN)_6]$ (1:1) mixture as redox probe and recorded in the frequency range of 0.01 Hz to 100 kHz with an amplitude of 50 mV. PEC measurements were carried out with a homemade PEC system. A 500W Xe lamp was used as the irradiation source with the light intensity of 400 $\mu W{\cdot}cm^{-2}$ estimated by a radiometer (Photoelectric Instrument Factory of Beijing Normal University). Photocurrent was recorded on a CHI 660D electrochemical workstation (Shanghai Chenhua Apparatus Corporation, China), and ITO modified electrode, saturated Ag/AgCl electrode, and platinum wire were used as working, reference, and counter electrode in this work, respectively. All PEC measurements were carried out in PBS (pH 8.0, 0.1 M) containing 10 mM AAP at room temperature with 0 V applied potential. The electrolyte solution was pumped into pure nitrogen for 10 min before PEC measurements.

Preparation of GR-CdS:Mn. A series of GR-CdS:Mn nanocomposites were prepared using the method according to the literature with some modifications.[19,20] Briefly, grapheme oxide (GO) sheets were prepared by a modified Hummers method[22] and then dispersed into water to yield a yellow brown dispersion by ultrasonication for 2 h, followed by centrifugation at 3000 rpm for 20 min to remove unexfoliated GO. In order to prepare GR-CdS:Mn nanocomposites, GO solution (150 μL, 0.8 mg mL^{-1}) and 0.2 g of PVP were dispersed into water (40 mL). After vigorous stirring, 0.114 g of $CdCl_2{\cdot}2.5H_2O$ and different concentrations of $Mn(Ac)_2{\cdot}4H_2O$ (0.5−7%, molar ratio of Mn:Cd) were added. The mixture was stirred magnetically at 80 °C until a homogeneous solution was obtained. Then, the corresponding amount of TAA was added into the mixture solution. The obtained solution was reacted at 80 °C for 2 h under vigorous stirring to form an orange GR-CdS:Mn solution. Finally, the product was centrifuged at 9000 rpm and dried in a vacuum drier. The GR sheets reduced by TAA, bare CdS NPs, free CdS:Mn NPs, and GR-CdS nanocomposites were also prepared under the same reaction conditions without adding $CdCl_2{\cdot}2.5H_2O$, $Mn(Ac)_2{\cdot}4H_2O$, or GO, respectively.

Fabrication of PEC Biosensor. The ITO slices were used as the working electrode, which were washed by immersing in acetone, ethanol/NaOH mixed solution (v/v, 1:1), and water, respectively, followed by drying at 60 °C for 2 h. Then, 20 μL of the GR-CdS:Mn solution (the molar ratio of Mn/Cd is 2%, 3 mg/mL) was dropped onto a piece of ITO slice with fixed area of 0.25 cm^2. Subsequently, the ITO/GR-CdS:Mn/ZnS modified electrode was fabricated by alternatively dipping ITO/GR-CdS:Mn electrode in 0.1 M $Zn(NO_3)_2{\cdot}6H_2O$ and 0.1 M Na_2S solution (1 min each) with intermediate methanol washings until the desired number of ZnS layers were assembled onto the ITO/GR-CdS:Mn substrate.[23] Then, the ITO/GR-CdS:Mn/ZnS modified electrode was immersed in 0.5 mL of 0.1 M Tris−HCl buffer (containing 0.1 M NaCl and 3 mM MPA) for 5 h at 4 °C.[24] After that, the ITO/GR-CdS:Mn/ZnS modified electrodes were immersed in a solution containing 10 mM EDC and 20 mM NHS for 30 min at room temperature, followed by washing with 10 mM Tris−HCl (pH 7.4) for three times. Then, 20 μL of pDNA suspension (1 μM) was casted onto the ITO/GR-CdS:Mn/ZnS electrode surface for 12 h under humid conditions, followed by rinsing with 10 mM Tris−HCl (pH 7.4) for three times, and pDNA could be conjugated onto as-prepared electrode by EDC-NHS coupling reactions between −COOH groups of MPA and the $-NH_2$ groups of pDNA. The obtained electrode was noted as ITO/

DOI: 10.1021/acs.analchem.5b00679
Anal. Chem. XXXX, XXX, XXX−XXX

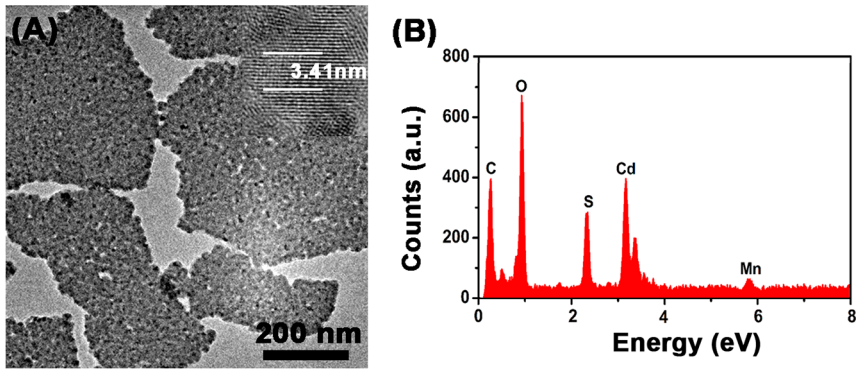

Figure 1. TEM image of the (A) GR-CdS:Mn nanocomposites; the inset is the HRTEM image of GR-CdS:Mn. (B) EDX spectra of GR-CdS:Mn nanocomposites.

GR-CdS:Mn/ZnS/pDNA. DNA hybridization was performed by incubating the ITO/GR-CdS:Mn/ZnS/pDNA electrode with 20 μL of tDNA hybridization buffer containing various concentrations of tDNA for 2 h at 37 °C. After being rinsed with 10 mM Tris−HCl (pH 7.4) for three times, the electrode was immersed in TdT extension solution (20 mM Tris−HCl, 50 mM KAc, 10 mM $Mg(Ac)_2$, 0.25 mM $CoCl_2$, pH 7.9, 200 U/mL TdT, 10 μM dUTP-biotin) and incubated at 37 °C for 80 min, followed by rinsing with 10 mM Tris−HCl (pH 7.4) for three times. Then, 20 μL of Av-ALP solution was added onto the electrode surface and incubated at 37 °C for 60 min. The electrode was rinsed with 10 mM Tris−HCl (pH 7.4) for three times and dried with nitrogen.

RESULTS AND DISCUSSION

Morphology and Spectroscopic Characterizations. Figure 1A shows the typical TEM image of the GR-CdS:Mn nanocomposites, indicating that all the GR sheets were densely and evenly decorated with CdS:Mn NPs. Neither free GR sheets nor undecorated CdS:Mn NPs could be observed in this sample. The good distribution and high coverage of CdS:Mn NPs on the GR sheets could guarantee the excellent optoelectronic properties of the GR-CdS:Mn nanocomposites. In the HRTEM image as shown in the inset of Figure 1A, the lattice fringe had an interplanar distance of 0.34 nm, which could be assigned to the (111) plane of the cubic CdS. Figure 1B shows the energy dispersive X-ray spectrum of the GR-CdS:Mn nanocomposites. The strong peaks for Cd and S were found in the spectrum. In addition, a detectable amount of Mn element in the spectrum indicated that Mn ions were successfully doped into the CdS NPs (the ratio of Mn/Cd is about 2.1%).

Figure S1A, Supporting Information, shows the UV/vis absorption spectra of the pristine GO, TAA-reduced GR, GR-CdS and GR-CdS:Mn nanocomposites. Pristine GO showed a strong absorption peak at 230 nm (curve a), whereas GR showed a characteristic peak at 270 nm (curve b), which was generally regarded as the excitation of the π−plasmon of graphitic structure.[25] The GR-CdS nanocomposites showed a broad peak at around 450 nm (curve c). However, as shown in Figure S1A, curve e, Supporting Information, the ZnS nanoparticles shell could not increase the absorption at the visible light wavelength range. Compared with the GR-CdS nanocomposites, the introduction of Mn ions could expand the visible absorption range from 500 to 800 nm (curves d and e). The enhanced visible absorption intensity is beneficial for the enhancement of the PEC property of the GR-CdS:Mn nanocomposites at the visible light wavelength range. Furthermore, the disappearance of the GO absorption peak (at about 230 nm) in curves c and d also indicated the reduction of GO to GR.[19]

An X-ray diffraction (XRD) measurement was conducted to investigate the phase and structure of the materials. As shown in Figure S1B, Supporting Information, the XRD pattern of GO showed a strong and sharp diffraction peak at 2θ of 10.61° (curve a), consistent with the lamellar structure of GO. For the obtained GR reduced by TAA, the strong diffraction peak disappeared and a weak and broad peak was observed at 2θ of 26.0° (curve b), indicating the reduction of GO to GR. The XRD pattern of the GR-CdS composites (curve c) only showed the peaks of the hexagonal CdS phase (JCPDS PDF 6-0314). The GR-CdS:Mn nanocomposites showed peaks at 2θ values of 28.5°, 45.9°, and 54.1°, which could be attributed to the (111), (220), and (311) crystal planes of cubic CdS, respectively (curve d). However, the peak for the GR could not be detected in the GR-CdS and GR-CdS:Mn nanocomposites, which may be ascribed to the relatively low diffraction intensity of GR and the masking effect of the CdS peak.[26]

FT-IR analysis was conducted to obtain further evidence of the reduction of GO to GR. Figure S1C, Supporting Information, shows the characteristic bands of GO of 1736, 1386, and 1226 cm^{-1} (curve a), which corresponded to the C═O stretching vibrations of the carboxyl or carbonyl groups, carboxyl O−H stretching, and phenolic C−OH stretching, respectively.[27] The peak at 1620 cm^{-1} was related to the H−O−H bending band of the adsorbed H_2O molecules or the in-plane vibrations of sp^2-hybridized C−C bonding.[28] Meanwhile, in the FT-IR spectra of GR, GR-CdS and GR-CdS:Mn nanocomposites (curves b, c, and d, respectively), almost all of the bands related to the oxygen-containing groups of GO decreased or disappeared, revealing that the oxygen-containing functional groups of GO were almost reduced by TAA.[29]

Raman spectroscopy is a powerful nondestructive tool to characterize the crystalline quality of carbon. Figure S1D, Supporting Information, shows the Raman spectra of pristine GO, GR reduced by TAA, GR-CdS and GR-CdS:Mn nanocomposites. Pristine GO (curve a) displayed two prominent peaks: ~1350 and ~1610 cm^{-1}, which corresponded well to the well-documented D and G band, respectively.[30,31] For the GR sheets, GR-CdS and GR-CdS:Mn nanocomposites (curves b, c, and d), in comparison to GO, the characteristic peaks of the D band moved to 1326 cm^{-1} while that of the G band shifted to 1597 cm^{-1}, indicating the reduction of GO. Moreover, the intensity ratio of the D/G band is also evidence

DOI: 10.1021/acs.analchem.5b00679
Anal. Chem. XXXX, XXX, XXX−XXX

of the relative concentration of local defects or disorders (particularly the sp^3-hybridized defects) compared with the sp^2-hybridized GR domains.[32,33] The D/G ratio of the GR sheets, GR-CdS and GR-CdS:Mn nanocomposites significantly decreased compared with that of pure GO, indicating the decrease in the average size of the sp^2 domains upon the reduction of GO to GR.[34,35]

Photoelectrochemical Properties of GR-CdS:Mn Nanocomposites. To investigate the photoelectrochemical properties of GR-CdS:Mn nanocomposites, the photocurrent of bare CdS NPs, free CdS:Mn NPs, GR-CdS and GR-CdS:Mn nanocomposites were measured. Figure S2, Supporting Information, shows the photocurrent of CdS NPs, CdS:Mn NPs, GR-CdS and GR-CdS:Mn nanocomposites in 10 mM AAP solution (Figure S2, Supporting Information). The photocurrent intensity of the GR-CdS:Mn nanocomposites was the strongest, which was about 2.5 times that of the CdS NPs. Because the doped Mn ions could trap electrons, the enhanced photocurrent intensity may improve the electron−hole pairs' life and enhance the visible light absorption intensity. Furthermore, the introduction of graphene could facilitate the spatial separation of charge carrier, thus, result in enhanced photocurrent intensity.[20,36]

As a wide band gap semiconductor, ZnS could be used as a passivation shell to reduce the number of surface defect states of the CdS NPs and avoid the recombination of charge carriers.[20,37] The thickness of the ZnS shell greatly influenced the photoelectric properties of the NPs, as shown in Figure S3, Supporting Information. When the ITO/GR-CdS:Mn electrodes were finally coated with two layers of ZnS, the corresponding photocurrent achieved a maximum value. Therefore, the ITO/GR-CdS:Mn/ZnS photoelectrode was used for the fabrication of the PEC DNA sensor.

PEC and EIS Characterization of the PEC DNA Assay. The fabrication of the PEC biosensor was monitored by photocurrent in 0.1 M PBS (pH 8.0) containing 10 mM AAP. As illustrated in Figure 2, after the GR-CdS:Mn/ZnS nanocomposites were modified on the ITO electrode, a weak photocurrent was observed (curve a), which can be ascribed to the absence of an efficient electron donor. The photocurrent decreased with the assembly of DNA sequence (curve b). The decrease in photocurrent may be attributed to the immobilized oligonucleotides, which increases the effect of steric hindrance and decreases the electron-transfer efficiency. However, the electrode exhibited an enhanced response with the immobilization of Av-ALP through specific interaction between avidin and biotin (curve c). The increase in photocurrent could be attributed to the generation of AA (electron donor) by the ALP enzyme, which could capture the photogenerated holes and improve the photocurrent response.[20,21]

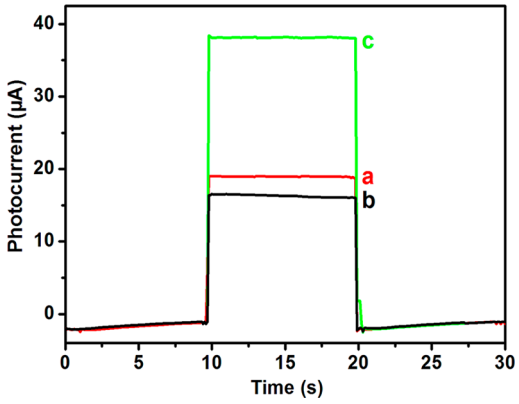

Figure 2. Photocurrent response of the different modified ITO electrodes in 0.1 M PBS (pH 8.0) containing 10 mM AAP: (a) GR-CdS:Mn/ZnS; (b) GR-CdS:Mn/ZnS/pDNA/tDNA(1 nM)/dUTP-TdT; (c) GR-CdS:Mn/ZnS/pDNA/tDNA (1 nM)/dUTP-TdT/Av-ALP for a catalysis time of 30 min.

Electrochemical impedance spectroscopy (EIS) is an effective method to obtain further information on the modified electrode surface. In EIS, the semicircle diameter at higher frequencies corresponds to the electron-transfer resistance (R_{et}), while the linear part at lower frequencies corresponds to the diffusion process. Figure S4, Supporting Information, shows the Nyquist plots of the impedance spectrum corresponding to the different stages; the inset shows the applied equivalent circuit. The EIS of the bare electrode showed a straight line with a very small semicircle (curve a), indicating that $[Fe(CN)_6]^{4-/3-}$ could reach the electrode surface and exchange charge conveniently. After the modification of GR-CdS:Mn/ZnS nanocomposites, the R_{et} significantly increased to 209.6 Ω (curve b), indicating that the nanocomposites were immobilized on the electrode surface and decreased the electron-transfer efficiency. When the electrode was assembled with pDNA (curve c) and tDNA (curve d), the R_{et} increased progressively to 293.4 and 457.8 Ω, respectively. The increased R_{et} value indicated that the electron transfer was obstructed by the assembled DNA strands, which blocked the redox electrochemical reaction of $Fe(CN_6)^{3-/4-}$. Subsequently, the dUTP-biotin was incorporated into the 3′-OH terminal of tDNA by TdT-mediated extension. A relatively larger semicircle could be observed (curve e, R_{et} = 523.2 Ω), indicating that $Fe(CN_6)^{3-/4-}$ had difficulty in reaching the electrode and exchanging charge with it. The Av-ALP was bound with the labeled biotin on the extended DNA sequence. The electrode showed a large increase in resistance (curve f, R_{et} = 733.5 Ω), suggesting that the ALP enzyme could form an additional barrier and further prevented the redox probe from reaching the electrode surface. These results showed that the proposed DNA biosensor was successfully fabricated.

Optimal Conditions for the Fabrication of PEC DNA Assay. The TdT-mediated dUTP-biotin extension reaction time is an important influence factor for the sensitivity of the PEC biosensor. Thus, the effect of incubation time on the photocurrent intensity was investigated. The photocurrent successively increased until 80 min and then reached a plateau, indicating that 80 min was the optimal incubation time (Figure 3A).

The ALP enzyme could catalyze the hydrolysis of AAP to generate AA, an efficient electron donor, and thereby increase the photocurrent.[20,21] Thus, the optimal incubation time of Av-ALP could play a significant role in optimizing the photocurrent signal, which could be estimated by the photocurrent with different incubation times of ALP. As shown in Figure 3B, with the incubation time extended, more Av-ALP enzymes could bind to dUTP-biotin until the saturation point (~60 min) is reached. The result shows that 60 min is the optimal incubation time for the ALP enzyme.

The concentration of AAP is also one of the key factors for photocurrent response, directly determining the generated amount of AA through catalytic hydrolysis of the ALP enzyme. Figure 3C shows that, with the increase in the AAP concentration, the photocurrent increased rapidly at lower

DOI: 10.1021/acs.analchem.5b00679
Anal. Chem. XXXX, XXX, XXX−XXX

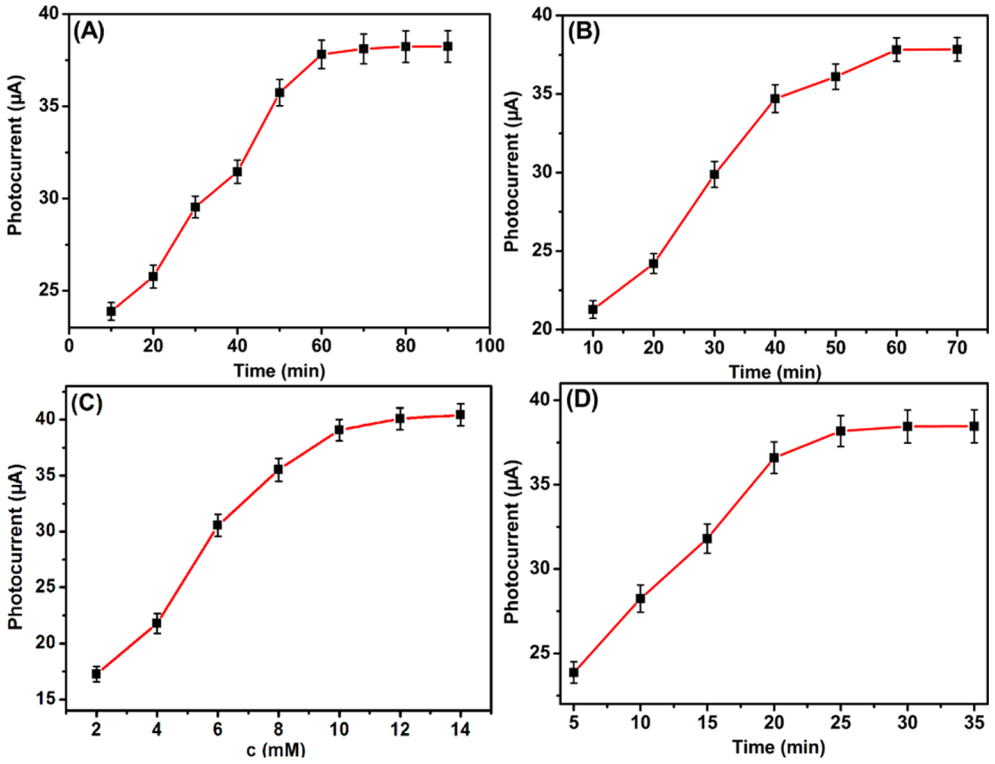

Figure 3. Influence of different reaction parameters on the photocurrent response of the ITO/GR-CdS:Mn/ZnS electrode. (A) The time of TdT-mediated dUTP-biotin extension reaction (200 U/mL TdT, 10 μM dUTP-biotin); (B) Av-ALP incubation time; (C) the concentration of AAP; (D) the time of ALP enzyme catalysis.

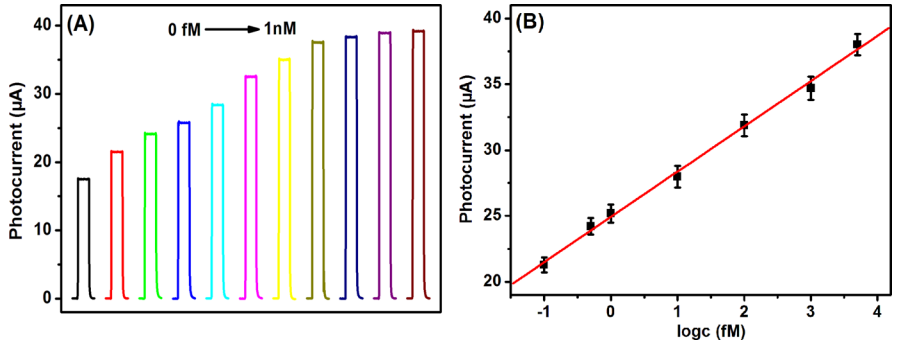

Figure 4. (A) Photocurrent response of the biosensor to different concentrations of HTLV-II DNA in 0.1 M PBS (pH 8.0) containing 10 mM AAP. The concentrations of tDNA were 0, 0.1, 0.5, 1, 10, 100, 1000, and 5000 fM, 100 and 500 pM, and 1 nM, respectively. (B) The linear calibration curve of the DNA biosensor for detection of different concentrations of HTLV-II DNA. Error bars represent standard deviations of measurements (n = 5).

concentration and then increased slowly above 10 mM. Thus, the AAP concentration of 10 mM was chosen as the final condition in the later measurement.

To achieve the "signal-on" strategy, AAP was enzymatically hydrolyzed by ALP to produce AA (electron donor). The formation of AA was a time-dependent process; thus, the reaction time of the enzymatic hydrolysis of AAP by ALP had a great influence on the performance of the fabricated biosensor.[20,21] Figure 3D shows the effect of ALP catalysis time on the photocurrent response of the modified electrode. More AA could be generated to capture the photogenerated holes and improve the photocurrent response with longer catalysis time. The photocurrent increased quickly with catalysis time of 25 min but increased slightly above 30 min. The results revealed that 30 min was the appropriate enzyme catalysis time.

Calibration Curve of the PEC Biosensor. The photocurrent response of the PEC DNA assay was found to be dependent on the immobilized amount of ALP enzyme, which was related to the concentration of tDNA (HTLV-II DNA). Upon treatment of the PEC assay with increasing tDNA, more ALP enzyme would bind on the DNA chains to result in the generation of more AA. That is, the PEC biosensor shows a linear relationship between photocurrent variation and the logarithm of tDNA concentration. Figure 4A depicted the photocurrent after the hybridization with various concentrations of tDNA. The photocurrent increased with increasing tDNA concentration. As shown in Figure 4B, the photocurrent was proportional to the logarithm of the tDNA concentration in a wide linear range of 0.1−5000 fM, with the linear regression equation of I (μA) = 24.93 + 3.44 log [c] (fM) and a correlation coefficient of 0.9985. The detection limit was 0.033

DOI: 10.1021/acs.analchem.5b00679
Anal. Chem. XXXX, XXX, XXX−XXX

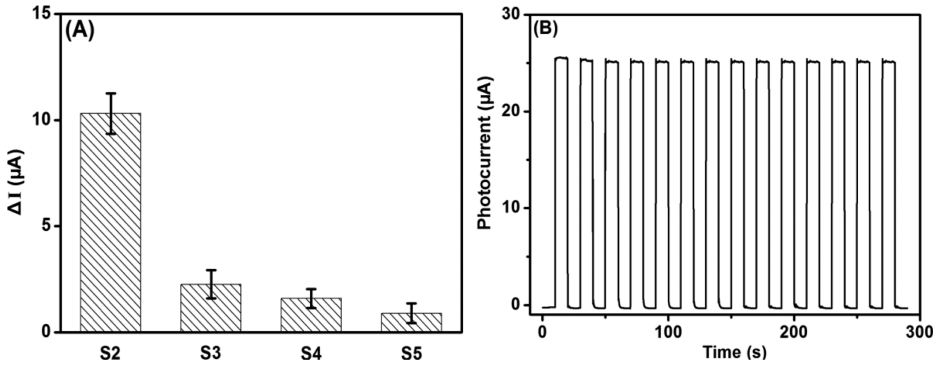

Figure 5. (A) Selectivity of the biosensor toward tDNA (S2) and base-mismatched target DNA (S3, S4, and S5). The concentration of DNA S2, S3, S4, and S5 were all 10.0 fM. (B) Time-based photocurrent responses of the PEC biosensor toward 1.0 fM tDNA in 0.1 M PBS (pH 8.0) containing 10 mM AAP.

fM at a signal-to-noise ratio of 3. The present biosensor showed high sensitivity and wide linear response range for the detection of DNA, which is better than the previous results.[38−41]

Selectivity, Reproducibility, and Stability of the PEC Biosensor. For the HTLV-II DNA biosensor, the detection specificity is an important parameter. To prove the detection specificity of the developed method, the photocurrent change of different hybridization models, complementary (S1−S2), one-based mismatch (S1−S3), three-based mismatch (S1−S4), and noncomplementary (S1−S5), was investigated, where the concentrations for base-mismatch DNA (S3, S4, and S5) and tDNA (S2) were all 10 fM. As shown in Figure 5A, the differences between the electrodes with different hybridization models were obvious. Although the photocurrent of the single-base mismatch DNA (S3) also could be observed (ΔI = 2.48 μA), it was not comparable with that of the tDNA (S2) (ΔI = 10.19 μA). The results demonstrated that the photocurrent response was specifically enhanced by the tDNA-triggered TdT-mediated extension and the enzyme amplification of ALP, indicating that the proposed DNA assay could offer high specificity.

The reproducibility of the PEC biosensor was evaluated by analyzing five independently prepared biosensors. By assaying toward 1.0 fM tDNA with five electrodes, a relative standard deviation (RSD) of 5.3% was obtained. The results indicated that the fabricated PEC biosensor has a satisfactory acceptable precision and reproducibility. The stability of the assay was examined by performing the detection of 1.0 fM tDNA. As shown in Figure 5B, no obvious change of photocurrent response could be observed for 300 s, indicating a good stability of the PEC DNA assay. In addition, the GR-CdS:Mn nanocomposites electrode shows a good stability, even after it was stored at 4 °C in dark conditions for 10 days (Figure S5, Supporting Information).

CONCLUSIONS

We described a novel sensitive PEC assay for HTLV-II DNA. The PEC assay was based on a dual signal amplification strategy, which combined enzymatic amplification with TdT-mediated extension. The intensity of the photocurrent signal was proportional to the concentration of HTLV-II DNA. On the basis of the novel strategy, the PEC assay could determine as low as ∼0.033 fM of HTLV-II DNA with a linear range of 0.1−5000 fM. The assay was relatively impervious to false signals because of the nonspecific adsorption of interfering agents. The developed PEC assay could be an attractive candidate for trace level DNA detection and supply valuable information for early clinical diagnosis.

ASSOCIATED CONTENT

Supporting Information

Additional information as noted in text. This material is available free of charge via the Internet at http://pubs.acs.org/.

AUTHOR INFORMATION

Corresponding Authors

*E-mail: jianglp@nju.edu.cn.
*E-mail: jjzhu@nju.edu.cn.

Notes

The authors declare no competing financial interest.

ACKNOWLEDGMENTS

We are grateful to the support of National Natural Science Foundation of China (21105050, 21475057), National Basic Research Program of China (2011CB933502), Program for New Century Excellent Talents in University (NCET-12-0256), Ministry of Education of China (No. IRT1148), Synergetic Innovation Center for Organic Electronics and Information Displays, and a project funded by the Priority Academic Program Development of the Jiangsu Higher Education Institutions.

REFERENCES

(1) Kalyanaraman, V. S.; Sarngadharan, M. G.; Robert-Guroff, M.; Miyoshi, I.; Golde, D.; Golde, R. C. *Science* **1982**, *218*, 571−573.
(2) Roucoux, D. F.; Murphy, E. L. *AIDS Rev.* **2004**, *6*, 144−54.
(3) Ho, D. D.; Moudgil, T.; Alam, M. *N. Engl. J. Med.* **1989**, *321*, 1621−1625.
(4) Erlich, H. A.; Gelfand, D.; Sninsky, J. J. *Science* **1991**, *252*, 1643−1651.
(5) Chen, C. F.; Ridzon, D. A.; Broomer, A. J.; Zhou, Z. H.; Lee, D. H.; Nguyen, J. T.; Xu, M. B.; Mahuvakar, N. L.; Mahuvakar, V. R.; Andersen, M. R.; Lao, K. Q.; Livak, K. J.; Guegler, K. J. *Nucleic Acids Res.* **2005**, *33*, e179.
(6) Mahmoudian, L.; Kaji, N.; Tokeshi, M.; Nilsson, M.; Baba, Y. *Anal. Chem.* **2008**, *80*, 2483−2490.
(7) Murakami, T.; Sumaoka, J.; Komiyama, M. *Nucleic Acids Res.* **2009**, *37*, e19.
(8) Wang, D. C.; Hu, L. H.; Zhou, H. M.; Abdel-Halim, E. S.; Zhu, J. J. *Electrochem. Commun.* **2013**, *33*, 80−83.
(9) Yan, J. I.; Li, Z. P.; Liu, C. H.; Cheng, Y. Q. *Chem. Commun.* **2010**, *46*, 2432−2434.

DOI: 10.1021/acs.analchem.5b00679
Anal. Chem. XXXX, XXX, XXX−XXX

(10) Li, C. P.; Li, Z. P.; Jia, H. X.; Yan, J. I. *Chem. Commun.* **2011**, *47*, 2595−2597.
(11) Notomi, T.; Okayama, H.; Masubuchi, H.; Yonekawa, T.; Watanabe, K.; Amino, N.; Hase, T. *Nucleic Acids Res.* **2000**, *28*, No. e63.
(12) Vet, J. A. M.; Majithia, A. R.; Marras, S. A. E.; Tyagi, S.; Dube, S.; Poiesz, B. J.; Kramer, F. R. *Proc. Natl. Acad. Sci. U.S.A.* **1999**, *96*, 6394−6399.
(13) Tjong, V.; Yu, H.; Hucknall, A.; Rangarajan, S.; Chilkoti, A. *Anal. Chem.* **2011**, *83*, 5153−5159.
(14) Wu, H. W.; Liu, S. C.; Jiang, J. H.; Shen, G. L.; Yu, R. Q. *Chem. Commun.* **2012**, *48*, 6280−6282.
(15) Fan, G. C.; Han, L.; Zhang, J. R.; Zhu, J. J. *Anal. Chem.* **2014**, *86*, 10877−10884.
(16) Wang, P.; Dai, W.; Ge, L.; Yan, M.; Ge, S.; Yu, J. *Analyst* **2013**, *138*, 939−945.
(17) Shen, Q. M.; Han, L.; Fan, G. C.; Abdel-Halimc, E. S.; Jiang, L. P.; Zhu, J. J. *Biosens. Bioelectron.* **2015**, *64*, 449−455.
(18) Fan, G. C.; Han, L.; Zhu, H.; Zhang, J. R.; Zhu, J. J. *Anal. Chem.* **2014**, *86*, 12398−12405.
(19) Zhao, X. M.; Zhou, S. W.; Jiang, L. P.; Hou, W. H.; Shen, Q. M.; Zhu, J. J. *Chem.—Eur. J.* **2012**, *18*, 4974−4981.
(20) Zhou, S. W.; Kong, Y.; Shen, Q. M.; Ren, X. L.; Zhang, J. R.; Zhu, J. J. *Anal. Chem.* **2014**, *86*, 11680−11689.
(21) Zhao, W. W.; Ma, Z. Y.; Yan, D. Y.; Xu, J. J.; Chen, H. Y. *Anal. Chem.* **2012**, *84*, 10518−10521.
(22) Hummers, W. S.; Offeman, R. E. *J. Am. Chem. Soc.* **1958**, *80*, 1339−1339.
(23) Li, T. L.; Lee, Y. L.; Tenq, H. *Energy Environ. Sci.* **2012**, *5*, 5315−5324.
(24) Shan, Y.; Xu, J. J.; Chen, H. Y. *Chem. Commun.* **2009**, 905−907.
(25) Wang, X.; Zhi, L. J.; Tsao, N.; Tomovic, J. L.; Mullen, K. *Angew. Chem., Int. Ed.* **2008**, *47*, 2990−2992.
(26) Li, Q.; Guo, B. D.; Yu, J. G.; Ran, J. R.; Zhang, B. H.; Yan, H. J.; Gong, J. R. *J. Am. Chem. Soc.* **2011**, *133*, 10878−10884.
(27) Szabo, T.; Tombacz, E.; Illes, E.; Dekany, I. *Carbon* **2006**, *44*, 537−545.
(28) Xu, Y. X.; Bai, H.; Lu, W.; Li, W.; Shi, G. Q. *J. Am. Chem. Soc.* **2008**, *130*, 5856−5857.
(29) Zhao, X. M.; Zhou, S. W.; Shen, Q. M.; Jiang, L. P.; Zhu, J. J. *Analyst* **2012**, *137*, 3697−3703.
(30) Xiang, Q. J.; Yu, J. G.; Jaroniec, M. *J. Phys. Chem. C* **2011**, *115*, 7355−7363.
(31) Stankovich, S.; Dikin, D. A.; Piner, R. D.; Kohlhaas, K. A.; Kleinhammes, A.; Jia, A.; Wu, Y.; Nguyen, S. T.; Ruoff, R. S. *Carbon* **2007**, *45*, 1558−15654.
(32) Zhang, Y. H.; Zhang, N.; Tang, Z. R.; Xu, Y. J. *ACS Nano* **2012**, *6*, 9777−9789.
(33) Liang, Y. T.; Vijayan, B. K.; Gray, K. A.; Hersam, M. C. *Nano Lett.* **2011**, *11*, 2865−2870.
(34) Zhou, K. F.; Zhu, Y. H.; Yang, X. L.; Jiang, X.; Li, C. Z. *New J. Chem.* **2011**, *35*, 353−359.
(35) Xiang, Q. J.; Yu, J. G.; Jaroniec, M. *Nanoscale* **2011**, *3*, 3670−3678.
(36) Santra, P. K.; Kamat, P. V. *J. Am. Chem. Soc.* **2012**, *134*, 2508−2511.
(37) Ai, H.; Hazelwood, K. L.; Davidson, M. W.; Campbell, R. E. *Nat. Methods* **2008**, *5*, 401−403.
(38) Zhang, X. R.; Su, H. R.; Bi, S.; Li, S. G.; Zhang, S. S. *Biosens. Bioelectron.* **2009**, *24*, 2730−2734.
(39) Yuan, L.; Tu, W. W.; Bao, J. C.; Dai, Z. H. *Anal. Chem.* **2015**, *87*, 686−692.
(40) Zhang, X. R.; Xu, Y. P.; Zhao, Y. Q.; Song, W. L. *Biosens. Bioelectron.* **2013**, *39*, 338−341.
(41) Wang, W. J.; Hao, Q.; Wang, W.; Bao, L.; Lei, J. P.; Wang, Q. B.; Ju, H. X. *Nanoscale* **2014**, *6*, 2710.

DOI: 10.1021/acs.analchem.5b00679
Anal. Chem. XXXX, XXX, XXX−XXX